Published in final edited form as:
Cancer Discov. 2011 July 22; 1(4): 352–365. doi:10.1158/2159-8290.CD-11-0106.

BIM expression in treatment naïve cancers predicts responsiveness to kinase inhibitors

Anthony Faber[1,2,*], **Ryan B. Corcoran**[1,2,*], **Hiromichi Ebi**[1,2,*], **Lecia V. Sequist**[1,2], **Belinda A. Waltman**[1,2], **Euiheon Chung**[3,Ω], **Joao Incio**[3], **Subba R. Digumarthy**[2,4], **Sarah F. Pollack**[1,2], **Youngchul Song**[1,2], **Alona Muzikansky**[1], **Eugene Lifshits**[1,2], **Sylvie Roberge**[3], **Erik J. Coffman**[1,2], **Cyril Benes**[1,2], **Henry Gómez**[5], **Jose Baselga**[1,2], **Carlos L. Arteaga**[6,7], **Miguel N. Rivera**[1,2,8], **Dora Dias-Santagata**[1,2,8], **Rakesh K. Jain**[3], and **Jeffrey A. Engelman**[1,2,#]

[1]Massachusetts General Hospital Cancer Center, Boston, MA 02129, USA

[2]Department of Medicine, Harvard Medical School, Boston, MA 02115, USA

[3]Radiation Oncology, Steele Lab for Tumor Biology, Massachusetts General Hospital and Harvard Medical School, Charlestown, MA 02129, USA

[4]Department of Radiology, Massachusetts General Hospital, Boston, MA 02114, USA

[5]Instituto Nacional de Enfermedades Neoplásicas, Lima, Perú

[6]Department of Medicine, Vanderbilt-Ingram Cancer Center, Vanderbilt University, Nashville, TN 37232, USA

[7]Breast Cancer Research Program, Vanderbilt-Ingram Cancer Center, Vanderbilt University, Nashville, TN 37232, USA

[8]Department of Pathology, Massachusetts General Hospital, Boston, MA 02114, USA

Abstract

Cancers with specific genetic mutations are susceptible to selective kinase inhibitors. However, there is wide spectrum of benefit among cancers harboring the same sensitizing genetic mutations. Herein, we measured apoptotic rates among cell lines sharing the same driver oncogene following treatment with the corresponding kinase inhibitor. There was a wide range of kinase inhibitor-induced apoptosis despite comparable inhibition of the target and associated downstream signaling pathways. Surprisingly, pre-treatment RNA levels of the BH3-only pro-apoptotic BIM strongly predicted the capacity of EGFR, HER2, and PI3K inhibitors to induce apoptosis in EGFR mutant, HER2 amplified, and PIK3CA mutant cancers, respectively, but BIM levels did not predict responsiveness to standard chemotherapies. Furthermore, BIM RNA levels in EGFR mutant lung cancer specimens predicted response and duration of clinical benefit from EGFR inhibitors. These findings suggest assessment of BIM levels in treatment naïve tumor biopsies may indicate the degree of benefit from single-agent kinase inhibitors in multiple oncogene-addiction paradigms.

Keywords

BIM; oncogene addiction; apoptosis; EGFR; HER2

[#]Address Correspondence to: Jeffrey A. Engelman, M.D., Ph.D., Massachusetts General Hospital Cancer Center, Building 149, 13th St, Boston, MA 02129, Phone: 617-724-7298, Fax: 617-724-9648, jengelman@partners.org.
[*]denotes equal contribution
[Ω]current address: Graduate-program of Medical System Engineering and School of Mechatronics Gwangju Institute of Science and Technology (GIST), Gwangju 500-712, Republic of Korea

Introduction

Subsets of cancers harboring specific genetic abnormalities are sensitive to specific kinase inhibitors. Two examples of these oncogene-addicted cancers include *EGFR* mutant lung cancers and *HER2* amplified breast cancers. In both cancer types, tyrosine kinase inhibitors (TKIs) or antibodies that disrupt the function of the corresponding receptor tyrosine kinase (RTK) are effective treatments (1–4). Other paradigms of oncogene addiction have more recently emerged, such as *EML4-ALK* translocated lung cancers treated with the ALK TKI critzotinib (5). Although these therapies are highly successful in these populations as a whole, there is a high degree of heterogeneity within each subtype. For example, although some patients benefit from a targeted therapy for much longer than one year, some only benefit for a few months. In addition, 30–40% of patients with *EGFR* mutant non-small lung cancers (NSCLCs) and *ALK* translocated lung cancers fail to achieve RECIST criteria responses to targeted therapy, for largely unknown reasons (5). The biology underlying this heterogeneity of clinical benefit is not well understood. In addition, biomarkers that identify those who do not benefit as greatly from single-agent targeted therapy would aid in directing them to novel therapeutic strategies.

The evasion of apoptosis is a hallmark of cancer and is often caused by disruptions in the intrinsic surveillance system regulating the survival of a cancer cell. Critical to this surveillance system is a group of Bcl-2 like proteins that connect growth factor signaling pathways with the mitochondria, the epicenter of apoptosis (6). In oncogene-addicted cancers, the growth and survival signals originating from the oncogene lead to the regulation of both the expression and the interactions of Bcl-2 family members. When the balance of pro- and anti-apoptotic proteins changes to favor apoptosis, as it often does following effective targeted therapy, two terminal members of the Bcl-2 family, Bak and Bax, homo- and/or hetero-dimerize to form porous channels in the mitochondria, committing the cell to apoptosis (6). Recent data has demonstrated that the pro-apoptotic Bcl-2 family member BIM is a particularly critical mediator of targeted therapy-induced apoptosis in both blood and solid tumor cancers (7–17). This BH3 only Bcl-2 family member directly binds to the antagonistic pro-apoptotic Bcl-2 members, such as Mcl-1 and Bcl-2, by binding into their hydrophobic clefts, countering their pro-survival effects (18). BIM also interacts directly with Bax, activating it to promote cell death (19).

In cancers addicted to receptor tyrosine kinases, the regulation of key intracellular signaling pathways (e.g., PI3K-AKT and MEK-ERK) is under strict control of the corresponding RTK. Pharmacological inhibition of the RTK with targeted therapies leads to suppression of these signaling pathways and often results in apoptosis (7,20–21). In *EGFR* mutant NSCLC cells, we and others have demonstrated that apoptosis is triggered by tipping the scale of pro- and anti-apoptotic Bcl-2 family members in favor of pro-apoptotic signaling (7–11). BIM levels increase following MEK-ERK pathway suppression, and Mcl-1 levels decrease following PI3K-mTORC pathway inhibition downstream of EGFR (7). Normally, the MEK-ERK pathway suppresses BIM expression by direct phosphorylation of BIM, leading to proteosomal degradation (22,23). The upregulation of BIM due to suppression of MEK-ERK signaling is essential for the induction of apoptosis, but in *EGFR* mutant cancers, it is not sufficient. Reducing levels of cellular BIM with siRNA and shRNA blocks TKI-induced apoptosis (7–11). Other successful targeted therapy paradigms have also demonstrated an integral role for BIM in promoting apoptosis in response to targeted therapies, including *BRAF* mutant colorectal cancers (13), *BRAF* mutant melanoma cancers (14,24,25), *Bcr-Abl* translocated chronic myeloid leukemia (CML) cancers (15), and *EML4-ALK* translocated lung cancers (26). Importantly, evidence from in vivo studies suggests, but does not prove, that the apoptotic response may be an essential contributor to marked tumor regressions in vivo upon treatment with targeted therapies (7,27). Thus, we hypothesize that patients with

oncogene-addicted cancers that undergo the most dramatic apoptotic responses to kinase inhibitors may enjoy the greatest benefit from kinase inhibitors. However, there has been no biomarker identified to date that accurately predicts which EGFR and HER2 addicted cancers are most likely to undergo robust apoptosis in response to to TKIs. Here, we describe the identification of pre-treatment BIM levels as a functional biomarker that predicts the induction of apoptosis in several oncogene-addiction paradigms. Assessment of this biomarker in clinical samples effectively distinguished the benefit that patients derived from single-agent EGFR TKIs.

Results

Pre-treatment BIM levels predicts apoptotic responses in EGFR mutant lung cancers treated with EGFR inhibitors

We were interested in studying cancers with disparate apoptotic responses to EGFR TKIs despite harboring the same activating *EGFR* mutation. Initially, we compared two *EGFR* mutant lung cancer cell lines, PC9 and HCC2279, that both harbor exon 19 deletions (Sup. Table 1). These two cell lines had markedly different apoptotic responses (PC9 ~65% vs. HCC2279 <10%) (Fig. 1A and Sup. Table 1 and Sup. Table 2), despite similar potent suppression of PI3K-AKT and MEK-ERK signaling following treatment with the EGFR TKI, gefitinib (Fig. 1B). Accordingly, EGFR TKIs led to a similar reduction in S phase cell cycle distribution in the two cell lines (Fig. 1C), consistent with the observed sensitivity of both cell lines to EGFR TKIs in short-term (72 hour) growth assays (28,29). In long-term growth assays, the growth of both cell lines was inhibited by gefitinib, but the cell viability of PC9 cells was impacted more than the HCC2279 cells (Fig. 1D), suggesting, but not proving, that the differential induction of apoptosis may even result in differences in growth in the presence of drug over long periods of time. To understand the differential apoptosis, we examined the regulation of the Bcl-2 family of proteins, and found that the expression of the pro-apoptotic extra long (EL) BIM protein (the most abundant form of BIM) was markedly diminished in HCC2279 cells compared to PC9 cells (Fig. 1E). Gefitinib increased the expression of BIM in both cell lines as expected due to MEK/ERK inhibition (~3 fold increase in PC9 cells and ~4 fold increase in HCC2279 cells) (7), but the level reached in HCC2279 cells remained substantially lower (~3 fold) than the level reached in PC9 cells (Fig. 1E).

These results raised the possibility that the pre-treatment and post-treatment levels of BIM might identify which cancer was most likely to undergo an apoptotic response following treatment with a TKI. Thus, we expanded these analyses to other *EGFR* mutant lung cancers. As shown in Fig. 2A, the cancers with the most pronounced apoptotic responses following gefitinib treatment tended to posses higher levels of BIM expression both pre-treatment ("− TKI") and post-treatment ("+TKI"). Of note, while gefitinib-treatment led to marked downregulation of PI3K-AKT and MEK-ERK signaling in seven of eight cell lines (Fig. 2A), the low BIM expressing H1650 cell line, which has a *PTEN* deletion, had retention of PI3K-AKT signaling in the presence of gefitinib (30). However, we found this cell line was also resistant to PI3K and MEK inhibitor combination therapy suggesting that resistance was due to more than just the loss of PTEN (Sup. Figs. 1A and 1B). Indeed, PI3K/MEK combination therapy is effective at inducing apoptosis in high BIM expressing cells but not in low BIM expressing cells (Sup. Fig. 1B and (7)) further supporting the notion that apoptotic responses to targeted therapies are blunted when cellular BIM levels are diminished.

Since BIM levels were induced by the TKI in all of the cell lines, this suggested that post-translational regulation of BIM was similar in all of the models. Thus, we hypothesized that the RNA levels might differ between the *EGFR* mutant cell lines that undergo pronounced

versus attenuated apoptotic responses. By performing quantitative RT-PCR, we found that RNA levels of BIM correlated with the magnitude of apoptosis (Fig. 2B, P=0.0018), suggesting RNA levels of BIM, like protein levels, predict apoptotic response to gefitinib in these cancers. However, we did not observe any correlation between BIM levels and induction of growth arrests as measured by a reduction in S phase (Sup. Fig. 1C), consistent with the downregulation of signaling in both low and high BIM expressing cell lines (Fig. 2A). Thus, it appears that BIM expression distinguishes apoptotic responses to EGFR inhibitors among these cell lines, but not the induction of growth arrest.

Pre-treatment BIM levels predict apoptotic responses in HER2 amplified cancers treated with HER2 inhibitors

We next investigated whether *HER2* amplified cancers, void of "hotspot" *PIK3CA* mutations, had differential rates of apoptosis following HER2 TKI (lapatinib) treatment. We first examined two *HER2* amplified breast cancer models, BT-474 and EFM-192A, treated with the HER2 TKI, lapatinib. There was a more pronounced induction of apoptosis in BT-474 cells compared to EFM-192A (~65% versus <5%) (Fig. 3A), although both cell lines downregulated phospho-HER2, PI3K/AKT and MEK/ERK signaling (Fig. 3B). The growth arrest induced by TKI was comparable in high and low expressing BIM lines (Fig. 3C), similar to the findings in the *EGFR* mutant cancer lines and consistent with the inhibition of signaling observed in both models (Fig. 3B). Long-term growth assays revealed that cell viability of BT-474 cells was impacted more than the EFM-192A cells (Fig. 3D). Although lapatinib increased the expression of BIM in both cell lines (as expected due to MEK/ERK inhibition), the level reached in EFM-192A cells was substantially lower (~6 fold) than levels reached in BT-474 cells (Fig. 3E). We extended these analyses to a panel of *HER2* amplified cancers. BIM was differentially expressed across the cell line panel. As shown in Fig. 4A, the cancers with the most pronounced apoptotic responses following lapatinib treatment possessed the highest levels of BIM expression both pre- and post-treatment. Importantly, none of these cell lines harbored *PIK3CA* hotspot mutations or *PTEN* loss that might impact sensitivity (Sup. Table 1). Accordingly, the intracellular signaling was suppressed in all cell lines (Fig. 4A). When BIM RNA expression was assessed in these cell lines by quantitative RT-PCR, BIM RNA levels correlated with the magnitude of apoptosis induced by lapatinib (Fig. 4A, P <0.0001). Of note, *HER2* copy number did not correlate with the magnitude of the apoptotic response (Sup. Table 1).

BIM levels predict apoptotic response in PIK3CA mutant and BRAF mutant cancers

In both *HER2* amplified and *EGFR* mutant cancers, treatment with the corresponding TKI increased BIM expression due to the suppression of MEK-ERK signaling, resulting in increased BIM stability (22,23). Similarly, we found that basal BIM levels predicted apoptotic response in ten *BRAF* mutant colorectal cell lines treated with the MEK inhibitor AZD6244, which effectively suppressed ERK phosphorylation in all of the models (Sup. Fig. 2 and Sup. Table 1). As with the HER2 and EGFR addicted models, pre-treatment levels of BIM RNA (P = 0.04) predicted AZD6244-induced apoptosis in *BRAF* mutant colorectal cells (Sup. Fig. 2B). We also evaluated whether basal levels of BIM predicted apoptosis in other oncogene-addicted cancers that did not rely on the ERK pathway for growth/survival. Thus, we examined the *PIK3CA* mutated cancers that are sensitive to PI3K inhibitors, and found that basal BIM RNA levels also indicated the apoptotic response to the PI3K-mTOR inhibitor NVP-BEZ235 in cancer cell lines harboring *PIK3CA* hotspot mutations (E545K and H1047R) (Fig. 4B). This was especially surprising since BIM decreased following treatment, possibly as a result of feedback activation of ERK signaling (7,31). Thus, BIM induction is not caused by PI3K inhibition, but its expression correlated with the magnitude of apoptosis suggesting that its basal expression is necessary in mediating the apoptotic response.

Apoptotic responses of oncogene-addicted cancers are predicated on BIM expression

While we and others have shown that knockdown of BIM expression abrogates the apoptotic response to EGFR and MEK inhibitors (7–11,13–14), it is unknown whether BIM mediates the apoptotic response to lapatinib in *HER2* amplified cancers and to PI3K inhibitors in *PIK3CA* mutated cancers. Since the findings above suggested a potential role in apoptosis in these cancer models as well, we reduced BIM levels using siRNA in *HER2* amplified BT-474 and SkBr3 cells and measured apoptosis following lapatinib treatment (Fig. 5A and Sup. Fig. 3A). *HER2* amplified breast cancer cells are also sensitive to single-agent PI3K inhibitors (7,27), and BIM knockdown accordingly protected from NVP-BEZ235-induced apoptosis (~ 60% reduction) in *HER2* amplified BT-474 and SkBr3 cells (Fig. 5A and Sup. Fig. 3A). Similarly, in cell lines with *PIK3CA* "hotspot" mutations, BIM knockdown protected cells from NVP-BEZ235 induced apoptosis compared to control cultures (Fig. 5B and Sup. Fig. 3B).

We next determined if BIM expression also protected from apoptosis induced by a cytotoxic chemotherapeutic, taxol (paclitaxel). We chose taxol because it is a clinically relevant chemotherapy for both lung and breast cancer. While apoptosis induced by gefitinib correlated with BIM expression in the *EGFR* mutant cancer cell lines (Fig. 2B), we found that taxol induced similar levels of apoptosis in low BIM and high BIM expressing cells (Fig. 5C). Accordingly, we observed that BIM knockdown provided a less impressive protective effect from taxol-induced apoptosis in the *HER2* amplified and *PIK3CA* mutated cancers, and reached statistical significance in only one of the four models tested (Fig. 5A, B and Sup. Fig. 3C). This suggests that the efficacy of the kinase inhibitors seem to be more sensitive to the amount of BIM in the cell than that of taxol. We also examined whether the amount of apoptosis induced by two other classic chemotherapies, the nucleoside analog gemcitabine, and the DNA cross-linker cisplatin, was abrogated following knockdown of BIM. We observed that BIM knockdown had a neglible impact on the ability of these two drugs to induce apoptosis in *HER2* amplified SkBr3 cells or *PIK3CA* mutant HCC1954 cells (Sup. Fig. 3D). Similar to the taxol analyses, BIM RNA levels did not predict apoptotic responses to either gemcitabine or cisplatin among *EGFR* mutant lung cancers (Fig. 5C). These data reveal that apoptosis induced by the targeted therapies are markedly more sensitive to BIM levels than apoptosis induced by the chemotherapies.

Induction of BIM expression can restore robust apoptotic responses in oncogene-addicted cancers

We determined whether induction of BIM expression could sensitize low BIM cancers to targeted therapies. We utilized tetracycline-on expression vectors that express BIM only in the presence of doxycycline, and used concentrations of doxycycline that lead to expression levels of BIM comparable to endogenous levels in high BIM expressing cells (Sup. Fig. 4). In H1650 *EGFR* mutant NSCLC cells and SKOV3 *PIK3CA* mutant ovarian cancer cells, adding doxycline in combination with the appropriate targeted therapy resulted in more pronounced apoptosis, as compared to cells that received targeted therapy alone (Sup. Fig. 4). These data suggest that restoration of BIM expression may re-sensitize some low BIM expressing oncogene-addicted cancers to targeted therapies.

Reducing BIM levels retards the apoptotic response and tumor shrinkage induced by EGFR TKI therapy

Since BIM levels in treatment naïve cells predicted for the amount of apoptosis induced by kinase inhibitors, we hypothesized that the level of apoptosis may correlate with clinical benefit. To directly determine if BIM-regulated apoptosis impacts tumor responsiveness in vivo, we utilized a BIM short hairpin (sh) sequence that is expressed only in the presence of doxycycline. When HCC827 cells were infected with scramble (SC) or BIM (shBIM)

inducible shRNA, we found only the shBIM cells were protected from gefitinib-induced apoptosis in the presence of doxycycline (Sup. Figs. 5A and 5B), which mitigated the decrease in cell culture number (Sup. Fig. 5C). The shBIM HCC827 cells were used to develop subcutaneous xenografts. Induction of BIM shRNA with doxcycyline led to reduced BIM levels in vivo and attenuated tumor regressions and apoptosis following gefitinib treatment (Fig. 6A and 6B and Sup. Fig. 5D). Thus, abrogation of apoptosis by BIM knockdown directly impacted the degree of tumor regression in vivo.

Consistent with the results that impairment of apoptosis by BIM knockdown mitigated tumor regressions in vivo, the high BIM expressing *HER2* amplified BT-474 cells were much more sensitive to lapatinib in vivo than the corresponding low BIM expressing ZR7530 cells (Figs. 6C and 6D) despite suppression of PRAS40 (i.e., AKT substrate) and ERK phosphorylation in vitro and in vivo in the ZR7530 cells (Sup. Fig. 6A and 6B). Since BIM levels and knockdown did not greatly impact taxol-induced apoptosis, we hypothesized that the combination of taxol and lapatinib in low BIM-expressing cells would yield greater anti-tumor effects than lapatinib alone by promoting both growth arrest and apoptosis, resulting in tumor regressions in vivo. Importantly, we did not observe that the addition of the TKI mitigated taxol-induced apoptosis in the low BIM expressing cells (Sup. Fig. 7A and 7B). Accordingly, the combination of lapatinib and taxol more potently induced ZR7530 tumor regressions in vivo (Sup. Fig. 7C), and this was associated with induction of apoptosis (Sup. Fig. 7D).

Patients with EGFR mutant NSCLCs with low BIM expression derive less clinical benefit from EGFR inhibitors

The above studies suggest that high BIM levels predict apoptotic response to TKIs and that this translates into more impressive and durable tumor responses in vivo. Thus, we aimed to determine if pre-treament BIM levels in patient samples would indicate clinical benefit to TKIs. We isolated nucleic acid from pre-treatment tumors in 24 patients with metastatic *EGFR* mutant lung cancers who received single-agent EGFR TKIs and assayed for BIM and β-actin RNA levels by quantitative RT-PCR. The patients consisted of 14 men and 10 women, with *EGFR* mutations including 13 exon 19 deletions, 9 L858R, 1 G719C and 1 L861Q. All cancers were void of T790M *EGFR* mutations, *KRAS* mutations, *PIK3CA* mutations or other known confounding genetic abnormality that would be expected to negatively impact response. The EMT status of these cancers was not known. Nineteen (79%) received the TKI in the first-line setting, the rest as the second systemic therapy for their cancer. Fifteen (62%) had high levels of BIM, defined as relative mRNA to β-actin >45, and nine (38%) had low levels of BIM, defined as relative mRNA to β-actin <30. BIM levels did not correlate with any particular type of *EGFR* mutation. Twenty-two of the twenty-four patients had scans available for quantification of responses. Fourteen patients (64%) achieved a RECIST response to TKI therapy, including 13 with partial responses (PR) and 1 with a complete response (CR). Using RECIST measurements, there was a significant correlation between BIM expression and tumor shrinkage. Low BIM patients had only a mean 29% tumor shrinkage, whereas high BIM patients achieved a mean 57% tumor decrease ($p=0.04$). Accordingly, the RECIST response rate was 44% amongst low BIM patients compared to 77% among high BIM patients (non-significant trend). The progression-free survival (PFS) was significantly different between the low and high BIM expressing patients (Fig. 7A) and the median PFS was only 4.7 months for the low BIM group versus 13.7 months for the high BIM group ($p=0.007$; Fig. 7A). We also developed BIM immunohistochemistry (IHC) using control cell lines with known low and high BIM levels (Sup. Fig. 8). In a few cases where tissue was available, we found that the BIM IHC intensity correlated well with qRT-PCR data (Fig. 7B).

Discussion

As the scientific and medical communities gain more experience with the effectiveness and limitations of targeted therapies in genetically defined cancers, it has become increasingly clear that there is significant heterogeneity among the clinical responses observed in the clinic even among cancers harboring the same genetic mutations. For example, roughly 30% of patients with *EGFR* mutant lung cancers from a recent clinical trial had modest or no tumor response to treatment with gefitinib (1). In this study, we have found that pre-treatment assessment of BIM levels in several different oncogene-addicted paradigms accurately predicts the apopototic response to targeted therapies. By comparing models with different levels of BIM and by knocking down expression of BIM in vivo, we observed that differential induction of apoptosis might be a strong contributing factor to tumor responsiveness in vivo. Upon assessment of BIM mRNA from a series of *EGFR* mutant lung cancers, we confirmed that BIM levels do serve as correlative marker for benefit from EGFR TKIs. Collectively, our data suggest that diminished expression of BIM, which is not only a biomarker for response, but also has critical function in the response, may contribute to the heterogeneity of responses observed in the clinic. Lack of BIM expression precludes the cell from undergoing robust apoptosis, which our data suggests is imperative for targeted therapies to impart robust and sustainable therapeutic responses.

The reasons for the heterogeneity in BIM expression remain poorly understood. In some cases, there may be genetic loss of BIM. For example, the *HER2* amplified Calu-3, *EGFR* mutant H1650, and *PIK3CA* mutant T47D and SKOV3 cells all have LOH at the BIM locus (32). Each of these models are low BIM expressors that fail to undergo robust apoptotic responses following targeted therapies (Figs. 2–4 and Sup. Table 1). There is also evidence from other liquid tumors that epigenetics may also contribute to suppression of BIM expression. Indeed, aberrant methylation of the BIM been associated with suppression of BIM expression and may contribute to resistance to targeted therapies among pediatric acute lymphoblastic leukemias (ALL), chronic myeloid leukemias (CML) and Burkitt Lymphoma (17, 33–36). In addition, suppression of BIM RNA levels via micro RNAs (mi-RNAs), including the miR-17–92 family (36), may also contribute to low basal BIM RNA levels. Since we found that re-expression of BIM re-sensitizes the cancers to targeted therapies, a more detailed understanding of the mechanisms of BIM suppression in these tumors may provide opportunities for therapeutic intervention to upregulate BIM in combination with the appropriate targeted therapy. An alternative strategy would be to add an apoptosis-inducing agent to the appropriate targeted therapy in low BIM expressing cancers. Since BIM expression did not substantially impact responsiveness to cytotoxics such as paclitaxel (this study), gemcitabine (this study) and cisplatinum (this study and 37,38), it may be advantageous to combine a cytotoxic agent (to achieve apoptosis) and a targeted therapy in low BIM expressing cancers. Such combinations are commonly used clinically in *HER2* amplified breast cancer; perhaps a similar approach could be utilized in low BIM expressing *EGFR*, *BRAF*, *EML4-ALK*, and *PIK3CA* mutant cancers that are currently treated with single-agent kinase inhibitors. Theoretically, combining the growth-arresting effect of the targeted therapy with a cytotoxic agent would mimic the growth-arresting and apoptosis-inducing activity achieved by single-agent targeted therapies in the high BIM expressors (Figs. 6C and 6D and Sup Fig. 7). Of note, the benefit of such combinations may be superior in the low BIM expressors in each specific oncogene-addiction paradigm and, in NSCLC, clinical trials have shown that this strategy is not successful when applied indiscriminately (39–41).

The studies in this manuscript also revealed that BIM expression is necessary for a robust apoptotic response following direct PI3K inhibition in *PIK3CA* mutant and *HER2* amplified cancers, and HER2 inhibition in *HER2* amplified cancers. To our knowledge, this had not

been reported previously. Indeed, over 70% of the BT-474 cells were protected from apoptosis by BIM siRNA following treatment with lapatinib or NVP-BEZ235 (Fig. 5A). To our initial surprise, BIM suppression blocked NVP-BEZ235-induced apoptosis in all cell lines studied, despite the lack of increase in BIM expression following PI3K-mTOR inhibition. Brachmann et al. showed NVP-BEZ235-induces apoptosis in *HER2* amplified and *PIK3CA* mutants through a caspase-dependent mechanism (27). We also have made similar observations in *HER2* amplified cancers (7,42), without detecting any reductions in Bcl-2 anti-apoptotic family members. In these experiments, we failed to detect any consistent decreases in Bcl-2, Bcl-xL or survivin following PI3K inhibition in the PIK3CA mutated cancers (Sup Fig. 9). Thus, these data suggest that BIM expression is necessary for apoptosis following PI3K inhibition, but apoptosis is not triggered by its expression *per se*. In the *HER2* amplified and *PIK3CA* mutant cancers, it seems likely that PI3K inhibition leads to alterations in other Bcl-2 family members (such as phosphorylation of BAD) that require basal BIM expression to promote apoptosis.

We have posited that low BIM expression in patient samples may help identify those with oncogene-addicted cancers that will not benefit as substantially from single-agent kinase inhibition. The in vivo xenograft data suggest apoptosis is a vital component of effective targeted therapy response, and that reductions in BIM expression are sufficient to impair tumor response (Fig. 6A). However, since it is more practical to clinically screen for BIM levels prior to treatment, it is important to note that cancers with low BIM expression before treatment were consistently the cancers that had the lowest BIM expression following treatments (Figs. 1–4, Sup. Fig. 2). Moreover, tumor samples from patients with *EGFR* lung cancers that displayed low BIM expression prior to gefitinib treatment predicted poor responses (Fig. 7). Similar results were observed in a small cohort of patients with HER2-overexpressing metastatic breast cancer enrolled in the only published study that used single-agent lapatinib (Sup. Fig.10) (43). While likely there are different processes cells undergo to diminish BIM during cancer progression, the resultant inadequate apoptotic response following targeted therapies translates into less pronounced patient responses. Our findings are supported by a recent study that found that patients with low BIM expression had poorer responses to imatinib in CML compared to those patients with higher BIM expression (35).

Given the complexity of cancer, it would be extremely unlikely that low BIM expression is the sole cause for diminished responsiveness or defective apoptosis in all cancers harboring genetic mutations suggesting oncogene addiction, despite the remarkable correlation among cell lines. Other factors, including inter-individual variability in drug pharmacokinetics and co-existing genetic changes are also likely contributing factors. It is also worthwhile to note other BH3 members play roles in the apoptotic response in oncogene-addicted cancers (44) and that even cancers with high BIM expression can have other impediments to the apoptotic response (45). Indeed, our patient data included cancers that had high BIM expression but tempered responses. Despite these possibilities, it is rather remarkable to us that BIM expression predicted for apoptotic response so effectively across oncogene-addiction models and may predict patient outcome. We also found it rather impressive that BIM expression levels serve as a functional biomarker across a wide range of kinase inhibitors and oncogene-addicted cancer models. Thus, it appears that apoptosis induced by inhibition of RTKs, PI3K-AKT, and MEK-ERK likely involves regulation of the Bcl-2 family members and requires BIM expression to effectively promote apoptosis. These data suggest that analyses of BIM expression in tumor samples before treatment regimens are selected for patients with these oncogene-addicted cancers may be merited. The next step would be to better understand why these cancers have diminished BIM expression in order to understand which combination therapy would be most suitable: therapies that may upregulate BIM expression (such as HDAC inhibitors or demethylating agents), therapies

that may induce apoptosis irrespective of BIM levels (cisplatin, gemcitabine or taxol), or therapies that may increase the amount of unbound BIM in the cell through targeting anti-apoptotic Bcl-2 family members, such as BH3 mimetics (46). Indeed, we are currently pursuing this line of investigation in the laboratory as a potential strategy to improve the efficacy of targeted therapies in cancers with low BIM expression.

Materials and Methods

Cell lines

BT-474, BT-20, SkBr3, Colo-201, Colo-205, Colo-206F, WiDr, RKO and SW1417 cells were cultured in DMEM/F12. The H3255 cells were cultured in ACL-4 media. All the rest of the cell lines in this study were cultured in RPMI. All the FBS concentrations were 10%, except for HCC827 cells (5%) and EFM-192A cells (20%). BT-474 and SkBr3 cells were from the Engelman laboratory and have been thoroughly characterized (7). MDA-MB-361, H1819 and MDA-MB-453 cells were provided by Dr. Carlos Arteaga (Vanderbilt-Ingram Cancer Center). The remaining *HER2* amplified, *PIK3CA* mutant and *BRAF* mutant cell lines were provided by the Center for Molecular Therapeutics (CMT) at Massachusetts General Hospital which performs routine cell line authentication testing by SNP and STR analysis. These cell lines have been acquired over the past 18 months. The *EGFR* mutant cell lines used in this study are from the Engelman laboratory and have been previously tested for mutation status to confirm their authenticity.

Antibodies and reagents

The following antibodies used for western blots were from Cell Signaling: BIM (catalog #2819), phospho-HER2, phospho-AKT (473), phospho-ERK, phospho pras40 (246), phospho-S6 (235/236), total HER2 and total ERK. Other antibodies were Actin (Sigma-Aldrich); phospho-EGFR 1068 (Abcam); and total EGFR and total AKT (Santa Cruz Biotechnology). Lapatinib was from LC laboratories and dissolved in DMSO. Taxol was from the pharmacy at MGH and diluted with saline. Gemcitabine was from Selleck Pharmaceuticals and dissolved in DMSO. Cisplatin was from Sigma-Aldrich and dissolved in water for immediate use. Antibodies used for immunohistochemistry are listed below.

Western blotting

For Western blotting, cells were prepared and lysed as previously described (7). Proteins were resolved using the NuPAGE® Novex® Midi Gel system on 4–12% Bis-Tris Gels (Invitrogen, Carlsbad, CA). Representative blots are shown from several experiments.

RNA extraction and quantitative (Q)RT-PCR

For cell lines, RNA was isolated and purified using the Quiagen RNeasy Mini kit and further purified by DNAse treatment with Ambion Turbo DNAse (47). For tumors, *EGFR* mutant lung and *HER2* positive breast tumor specimens were extracted prior to TKI treatment and were then paraffin embedded and mounted on glass slides. For *EGFR* mutant tumor tissue, total nucleic acid was extracted using a modified FormaPure System (Agencourt Bioscience Corporation, Beverly, MA) automated on a Beckman Couter Biomek NX^P workstation. For *HER2* positive tumors, RNA was extracted and purified from the slides using the Pinpoint Slide RNA Isolation System II (Zymo Research). Following extraction and purification, RNA was reverse transcribed and amplified using superscript First-strand cDNA synthesis (Invitrogen). The amplicon abundance of BIM and β-Actin was monitored in real time on a Roche Lightcycler 480 (Roche Diagnostics) by measuring the fluorescence increases of Sybr Green. The primers used for cell lines were: BIM Forward (5'-GATCCTTCCAGTGGGTATTTCTCTT-3') and BIM Reverse (5'-

ACTGAGATAGTGGTTGAAGGCCTGG-3'), β-Actin Forward (5'-CTGTGCTATCCCTGTACGCCTC-3') and β-Actin Reverse, (5'-CATGATGGAGTTGAAGGTAGTTTCGT-3'). For tumor samples, target amplicons were shortened to 60–80 base pairs. To avoid genomic DNA contamination, the BIM forward primer was designed to overlap exon 2 and exon 3 and specifically amplified BIM_{EL} cDNA. The primer pairs were: BIM Forward (5'-ATCTCAGTGCAATGGCTTCC-3') and BIM Reverse (5'-CAACTCTTGGGCGATCCATA-3'), and β-Actin Forward 5'-GGCATGGGTCAGAAGGATT-3') and β-Actin Reverse (5'-AGGATGCCTCTCTTGCTCTG-3'). Relative BIM RNA levels were calculated using the Delta-Delta threshold cycle (C_t) method as previously described (48). Threshold levels were set for the exponential phase of amplification as previously described (48).

In vitro and in vivo shRNA experiments

BIM short hairpin (SH) sequence (5'-ATGGTTATCTTACGACTGTTA-3') and scrambled (SC) SH sequence (5'-CCTAAGGTTAAGTCCGGGTCGAGCGAGGGCGACTTAACCTTAGG-3') were introduced into the tet-on PLKO vector. For the BIM SH studies, high BIM expressing HCC827 cells were infected with tet-on PLKO BIM SH and tet-on PLKO BIM SC knockdown vectors and selected for in 2ug/ul puromycin. For the in vivo experiments, HCC827 cells stably transduced with tet-on shBIM were injected into the left flanks of 6–8 week old male nu/nu nude mice (5×10^6 cells per mouse). Tumor size was measured every 3–4 days for 21 days. The perpendicular diameters of the tumors were measured using a caliper and the tumor volumes were calculated using the formula: $v = l \times (w)2 (\pi/6)$, where v = tumor volume, l = length of tumor and w = width of tumor. For the BIM SH studies, high BIM expressing HCC827 cells were infected with tet-on PLKO BIM SH and tet-on PLKO BIM SC knockdown vectors and selected for in 2ug/ul puromycin. For the in vivo experiments, HCC827 cells stably transduced with tet-on shBIM were injected into the flanks of nu/nu nude mice (5 × 10^6 cells per mouse). Once tumors reached an average volume of 100mm3, mice were randomized to receive control or doxycycline-containing chow, which was changed weekly. After 10–14 days, when tumors reached an approximate size of 750 mm3, mice were treated with 35mg/kg gefitinib (LC Laboratories) daily by oral gavage, as previously described (49). Mice were randomized to at least three per group.

siRNA experiments

For the siRNA experiments, BIM and negative control oligos (Quiagen) were used at a concentration of 10nM and transfected with HiperFect following the manufacturer's protocol (Quiagen) and as previously described (7).

Doxycycline (DOX)-inducible pTREX expression vectors

BIM_{EL} cDNA in the pDEST26 vector was generously provided by Dr. Hidesuke Fukazawa (Department of Bioactive Molecules, National Institute of Infectious Diseases, Tokyo, Japan) and the cDNA was introduced into the pTREX vector kindly provided by Novartis Pharmaceuticals (Basel, Swizerland). Briefly, the BIM sequence was amplified by PCR with the Forward Primer 5'-CACCATGGCAAGCAACCTTCTGATG-3'and Reverse Primer 5'-TCAATGCATTCTCCACACC-3' and cloned into pENTR using the TOPO Cloning method (Invitrogen). The sequence was then cloned into the pTREX vector by the clonase recombination reaction (Invitrogen). pTREX BIM vectors were subsequently verified by DNA sequencing at the MGH DNA Sequencing Core. The Low BIM expressing *EGFR* mutant H1650 NSCLC and *PIK3CA* mutant SKOV3 ovarian cancer cells were infected with pTREX BIM vectors, and selected in 1ug/ul puromycin in RPMI supplemented with 10% tetracycline-free FBS. When cells grew to confluency, cells were split and titrated with doxycyline (DOX). The purpose was to find a concentration of DOX that induced BIM to a

comparable level found in high BIM expressing cells. This concentration was subsequently used to see if this concentration of BIM sensitized the cells to the appropriate targeted therapy. For these experiments, cells were incubated with DOX for 24 hours, followed by treatment with vehicle or with the appropriate targeted therapy. Parallel cultures of cells were treated with vehicle or appropriate targeted therapy without pre-incubation with DOX.

Flow Cytometry

FACS analysis was performed on a BD LSR III (Becton Dickenson). For cell cycle studies and apoptosis measurements, experiments were carried out as previously described (48). The annexin Cy5 was from Biosource International (Camarillo, CA). Experiments were carried out in triplicate and standard deviations are shown (Sup. Table 1 and Sup. Table 2).

Patient Selection for EGFR mutant lung cancer data

The Massachusetts General Hospital (MGH) began screening patient tumors for EGFR mutations in 2004 and expanded the tumor genotyping platform to screen for additional oncogenic mutations in 2009 (50). We retrospectively collected a cohort of *EGFR*-mutant NSCLC patients seen in our Thoracic Oncology clinic between October 2005 and July 2010 via chart review under an IRB-approved protocol. To meet criteria for inclusion, patients had to have 1) documented *EGFR* mutation (exon 19 del, L858R, G719X or L861Q only, as these have been the most strongly associated with sensitivity to EGFR TKIs), 2) treatment with single agent EGFR TKI, without concurrent chemotherapy, other targeted agent, or radiation 3) sufficient baseline tissue available for analysis (baseline defined as resected or biopsied prior to initiation of EGFR TKI therapy), and 4) pre-treatment and post-treatment radiographic scans available for tumor measurements. Twenty-four patients ultimately met these criteria, all treated with either erlotinib or gefitinib except one who received a second-generation EGFR TKI, afatinib. Radiographs were centrally reviewed by a single radiologist (S.D.) who was blinded to BIM results. RECIST methods were used to determine standard overall tumor burden quantitative measurements at each time point (the sum of longest diameters of the target lesions) and best response as well as percent decrease from baseline was calculated (51). Time-to-progression (TTP) was calculated as the time from the start of EGFR TKI until documented progression by RECIST. Patients that did not progress were censored at their last known follow-up. If RECIST progression could not be documented because of lack of formal assessment by CT scan or unavailability of films from outside hospitals (n= 7), the date of progression as documented in clinical notes (n=6), or the start date of next therapy (n=1) was used. Best response to therapy was compared by BIM high versus low using the Wilcoxon rank sum test and Fisher's exact test and TTP was calculated with the Kaplan-Meier method and log-rank test. Low BIM levels were defined as relative mRNA to β-actin >45, and low levels of BIM, defined as relative mRNA to β-actin <30. The cut-off for the BIM RNA levels was empirical and chosen because there was a clear separation in values with all values being either below 30 or above 45 (i.e., there were no cancers with values between 30 and 45). This stratification profoundly distinguished patient outcomes, and changing the cut-offs did not improve the distinction in clinical outcomes.

Mammary Fat Pad Xenograft Studies

One week before tumor implantation, 6–8 week old (to be confirmed) nu/nu nude female mice underwent ovariectomy and were implanted subcutaneously with controlled release pellets containing 0.75 mg of estrogen for 60-day release (Innovative Research, Sarasota, FL). This allows enough time to recover from any estrogen depletion-induced, hemodynamic changes and limits any residual effect of endogenous estrogen, which may vary between, animals and potentially influence tumor growth rates. High BIM BT-474 (N=7/treatment group) or Low BIM ZR7530 (N=3/treatment group) *HER2* amplified tumor cells (approximately 3 × 10^6 in PBS) were mixed with high-concentration Matrigel (BD

Biosciences) at 1:1 ratio and the mixture was injected using a 30-gauge needle, under a dissecting microscope subcutaneously into the mammary fat pad just inferior to the 3rd nipple of the anesthetized, ovariectomized female mice. Leakage to subcutaneous space was avoided. Pellets were replenished approximately every 60 days during ongoing experimentation. Tumor size was measured as described above for HCC827 tumors. Once tumors reached an average volume of 100 mm^3, mice were treated with either vehicle, 100mg/kg lapatinib (once a day, oral gavage) and/or 10mg/kg paclitaxel (injected into mammary fat pad) for the indicated times.

Immunohistochemistry

Immunohistochemistry for tissue sections was performed using standard protocols with the following antibody dilutions, 1:100 BIM (Cell Signaling #2933), 1:100 phospho-ERK (Cell Signaling #4370), 1:200 phospho-Pras40 (Cell Signaling #2997), and 1:200 cleaved caspase 3 (CC3) (Cell Signaling #9661). Briefly, the sections were deparaffinized using Xylene, quenched with hydrogen peroxide, and antigen retrieval was performed using Borg Decloaking solution in a Decloaking Chamber (Biocare Medical). Subsequently, we incubated tissues with primary antibodies overnight followed by incubation with secondary antibodies for 1 hour at room temperature. Signals were detected using the ABC kit for immunoperoxidase staining (Vector laboratories). Images were taken by a Nikon 90i scope with color camera.

Statistical Analyses

Linear regression analyses, Student's *t* tests and Log-rank tests were performed when indicated and calculations were performed using GraphPad Software (San Diego, CA). For linear regression analyses, the slope was considered significantly non-zero when $P<0.05$. For Student's t tests and Log-rank tests, populations were considered significantly different at $P<0.05$.

Significance

In several oncogene-addiction paradigms, assessment of BIM RNA levels identifies those cancers that fail to have substantial apoptotic responses to kinase inhibitors. BIM RNA levels may be assessed in diagnostic cancer specimens to predict which patients will receive less benefit from single-agent kinase inhibitors.

Supplementary Material

Refer to Web version on PubMed Central for supplementary material.

Acknowledgments

The authors thank Elizabeth Bast for her help in collecting and analyzing the clinical data.

This study is supported by grants from the National Institutes of Health NIH R01CA137008-01 (J.A.E.), R01CA140594 (J.A.E), R01CA135257-01 (J.A.E.), National Cancer Institute Lung SPORE P50CA090578 (J.A.E), DF/HCC Gastrointestinal Cancer SPORE P50 CA127003 (J.A.E.), K08 grant CA120060-01 (J.A.E.), the American Lung Cancer Association Lung Cancer Discovery Award (J.A.E.), the V Foundation (J.A.E.), the Ellison Foundation Scholar (J.A.E.), and an Aid for Cancer Research Postdoctoral Fellowship (A.C.F.).

References

1. Sequist LV, Martins RG, Spigel D, Grunberg SM, Spira A, Jänne PA, et al. First-line gefitinib in patients with advanced non-small cell lung cancer harboring somatic EGFR mutations. J Clin Onc. 2008; 26:2442–2449.

2. Scaltriti M, Chandarlapaty S, Prudkin L, Aura C, Jimenez J, Angelini PD, et al. Clinical benefit of lapatinib-based therapy in patients with human epidermal growth factor receptor 2-positive breast tumors coexpressing the truncated p95HER2 receptor. Clin Canc Res. 2010; 16:2688–2695.
3. Lynch TJ, Bell DW, Sordella R, Gurubhagavatula S, Okimoto RA, Brannigan BW, et al. Activating mutations in the epidermal growth factor receptor underlying responsiveness of non-small-cell lung cancer to gefitinib. N Engl J Med. 2004; 21:2129–2139. [PubMed: 15118073]
4. Shaw AT, Yeap BY, Mino-Kenudson M, Digumarthy SR, Costa DB, Heist RS, et al. Clinical features and outcome of patients with non-small-cell lung cancer who harbor EML4-ALK. J Clin Onc. 2010; 26:4247–4253.
5. Kwak EL, Bang YJ, Camidge DR, Shaw AT, Solomon B, Maki RG, et al. Anaplastic lymphoma kinase inhibition in non-small-cell lung cancer. N Engl J Med. 2010; 18:1693–1703. [PubMed: 20979469]
6. Heath-Engel HM, Shore GC. Regulated targeting of Bax and Bak to intracellular membranes during apoptosis. Cell Death Differ. 2006; 13:1277–1280. [PubMed: 16710364]
7. Faber AC, Li D, Song Y, Liang MC, Yeap BY, Bronson RT, et al. Differential induction of apoptosis in HER2 and EGFR addicted cancers following PI3K inhibition. PNAS. 2009; 46:19503–19508. [PubMed: 19850869]
8. Costa DB, Halmos B, Kumar A, Schumer ST, Huberman MS, Boggon TJ, et al. BIM mediates EGFR tyrosine kinase inhibitor-induced apoptosis in lung cancers with oncogenic EGFR mutations. PLoS Med. 2007; 10:1669–1679. [PubMed: 17973572]
9. Cragg MS, Kuroda J, Puthalakath H, Huang DC, Strasser A. Gefitinib-induced killing of NSCLC cell lines expressing mutant EGFR requires BIM and can be enhanced by BH3 mimetics. PLos Med. 2007; 10:1681–1689. [PubMed: 17973573]
10. Deng J, Shimamura T, Perera S, Carlson NE, Cai D, Shapiro GI, et al. Proapoptotic BH3-only BCL-2 family protein BIM connects death signaling from epidermal growth factor receptor inhibition to the mitochondrion. Cancer Res. 2007; 67:11867–11875. [PubMed: 18089817]
11. Gong Y, Somwar R, Politi K, Balak M, Chmielecki J, Jiang X, et al. Induction of BIM is essential for apoptosis triggered by EGFR kinase inhibitors in mutant EGFR-dependent lung adenocarcinomas. PLoS Med. 2007; 10:e294. [PubMed: 17927446]
12. Rahmani M, Anderson A, Habibi JR, Crabtree TR, Mayo M, Harada H, et al. The BH3-only protein Bim plays a critical role in leukemia cell death triggered by concomitant inhibition of the PI3K/Akt and MEK/ERK1/2 pathways. Blood. 2009; 114:4507–4516. [PubMed: 19773546]
13. Wickenden JA, Jin H, Johnson M, Gillings AS, Newson C, Austin M, et al. Colorectal cancer cells with the BRAF(V600E) mutation are addicted to the ERK1/2 pathway for growth factor-independent survival and repression of BIM. Oncogene. 2007; 27:7151–7161.
14. Cragg MS, Jansen ES, Cook M, Harris C, Strasser A, Scott CL. Treatment of B-RAF mutant human tumor cells with a MEK inhibitor requires Bim and is enhanced by a BH3 mimetic. J Clin Invest. 2008; 118:3651–3659. [PubMed: 18949058]
15. Kuribara R, Honda H, Matsui H, Shinjyo T, Inukai T, Sugita K, et al. Roles of Bim in apoptosis of normal and Bcr-Abl-expressing hematopoietic progenitors. Mol Cell Biol. 2004; 14:6172–6183. [PubMed: 15226421]
16. Zhang W, Konopleva M, Ruvolo VR, McQueen T, Evans RL, Bornmann WG, et al. Sorafenib induces apoptosis of AML cells via Bim-mediated activation of the intrinsic apoptotic pathway. Leukemia. 2008; 22:808–818. [PubMed: 18200035]
17. Richter-Larrea JA, Robles EF, Fresquet V, Beltran E, Rullan AJ, Agirre X, et al. Reversion of epigenetically mediated BIM silencing overcomes chemoresistance in Burkitt lymphoma. Blood. 2010; 116:2531–2542. [PubMed: 20570860]
18. Willis SN, Fletcher JI, Kaufmann T, van Delft MF, Chen L, Czabotar PE, et al. Apoptosis initiated when BH3 ligands engage multiple Bcl-2 homologs, not Bax or Bak. Science. 2007; 15:856–859. [PubMed: 17289999]
19. Gavathiotis E, Suzuki M, Davis ML, Pitter K, Bird GH, Katz SG, et al. BAX activation is initiated at a novel interaction site. Nature. 2008; 455:1047–1049. [PubMed: 18948940]

20. Engelman JA, Jänne PA, Mermel C, Pearlberg J, Mukohara T, Fleet C, et al. ErbB-3 mediates phosphoinositide 3-kinase activity in gefitinib-sensitive non-small cell lung cancer cell lines. PNAS. 2005; 10:3788–3793. [PubMed: 15731348]
21. Engelman JA, Zejnullahu K, Mitsudomi T, Song Y, Hyland C, Park JO, et al. MET amplfication leads to gefitinib resistance in lung cancers by activating ERBB3 signaling. Science. 2007; 5827:1039–1043. [PubMed: 17463250]
22. Ley R, Balmanno K, Hadfield K, Weston C, Cook SJ. Activation of the ERK1/2 signaling pathway promotes phosphorylation and proteasome-dependent degradation of the BH3-only protein, Bim. J Biol Chem. 2003; 278:18811–18816. [PubMed: 12646560]
23. Fukazawa H, Noguchi K, Masumi A. BimEL is an important determinant for induction of anoikis sensitivity by mitogen-activated protein/extracellular signal-regulated kinase kinase inhibitors. Molec Cancer Ther. 2004; 5:303–309.
24. Flaherty KT, Puzanov I, Kim KB, Ribas A, McArthur GA, Sosman JA, et al. Inhibition of mutated, activated BRAF in metastatic melanoma. N Engl J Med. 2010; 9:809–819. [PubMed: 20818844]
25. Board RE, Ellison G, Orr MC, Kemsley KR, McWalter G, Blockley LY, et al. Detection of BRAF mutations in the tumour and serum of patients enrolled in the AZD6244 (ARRY-142886) advanced melanoma phase II study. BRJ Cancer. 2009; 101:1724–1730.
26. Takezawa K, Okamoto I, Nishio K, Janne P, Nakagawa K. Role of ERK-BIM and STAT3-survivin signaling pathways in EML4-ALK-positive lung cancer. Clin Cancer Res. 2011; 8:2140–2148. [PubMed: 21415216]
27. Brachmann SM, Hofmann I, Schnell C, Fritsch C, Wee S, Lane H, et al. Specific apoptosis induction by the dual PI3K/mTor inhibitoRNVP-BEZ235 in HER2 amplified and PIK3CA mutant breast cancer cells. PNAS. 2010; 52:22299–22234.
28. Mukohara T, Engelman JA, Hanna NH, Yeap BY, Kobayashi S, Lindeman N, et al. Differential effects of gefitinib and cetuximab on non-small-cell lung cancers bearing epidermal growth factor receptor mutations. J Natl Cancer Inst. 2005; 16:1185–1194. [PubMed: 16106023]
29. Zhou BB, Peyton M, He B, Liu C, Girard L, Caudler E, et al. Targeting ADAM-mediated ligand cleavage to inhibit HER3 and EGFR pathways in non-small cell lung cancer. Cancer Cell. 2006; 1:39–50. [PubMed: 16843264]
30. Janmaat ML, Rodriguez JA, Gallegos-Ruiz M, Kruyt FA, Giaccone G. Enhanced cytotoxicity induced by gefitinib and specific inhibitors of the Ras or phosphatidyl inositol-3 kinase pathways in non-small cell lung cancer cells. Int J Cancer. 2006; 118:2370.
31. Wang CC, Cirit M, Haugh JM. PI3K-dependent cross-talk interactions converge with Ras as quantifiable inputs integrated by Erk. Mol Syst Biol. 2009; 5:246–253. [PubMed: 19225459]
32. http://www.sanger.ac.uk/
33. Bachmann PS, Piazza RG, Janes ME, Wong NC, Davies C, Mogavero A, et al. Epigenetic silencing of BIM in glucocorticoid poor-responsive pediatric acute lymphoblastic leukemia, and its reversal by histone deacetylase inhibition. Blood. 2010; 9:4482–4490.
34. Jiang N, Koh GS, Suang Lim JY, Yin Kham SK, Ariffin H, Chew FT, et al. BIM is a prognostic biomarker for early prednisolone response in pediatric acute lymphoblastic leukemia. Exp Hemat. 2011; 39:321–329. [PubMed: 21130142]
35. San José-Eneriz E, Agirre X, Jiménez-Velasco A, Cordeu L, Martín V, Arqueros V, et al. Epigenetic down-regulation of BIM expression is associated with reduced optimal responses to imatinib treatment in chronic myeloid leukaemia. Eur J Cancer. 2009; 45:877–889.
36. Xiao C, Srinivasan L, Calado DP, Patterson HC, Zhang B, Wang J, et al. Lymphoproliferative disease and autoimmunity in mice with increased miR-17–92 expression in lymphocytes. Nat Immunol. 2008; 9:405–414. [PubMed: 18327259]
37. Li Z, Zhang J, Liu Z, Woo CW, Thiele CJ. Downregulation of Bim by brain-derived neurotrophic factor activation of TrkB protects neuroblastoma cells from paclitaxel but not etoposide or cisplatin-induced cell death. Cell Death Differ. 2007; 14:318–326. [PubMed: 16778834]
38. Bartling B, Hofmann HS, Silber RE, Simm A. Differential impact of fibroblasts on the efficient cell death of lung cancer cells induced by paclitaxel and cisplatin. Cancer Biol Ther. 2008; 7:1250–1261. [PubMed: 18487950]

39. Fuster LM, Sandler AB. Select clinical trials of erlotinib (OSI-774) in non-small-cell lung cancer with emphasis on phase III outcomes. Clin Lung Cancer. 2004; 6:S24–S29. [PubMed: 15638954]
40. Bell DW, Lynch TJ, Haserlat SM, Harris PL, Okimoto RA, Brannigan BW, et al. Epidermal growth factor receptor mutations and gene amplification in non-small cell lung cancer: molecular analysis of the IDEAL/INTACT gefitinib trials. J Clin Oncol. 2005; 23:8081–8092. [PubMed: 16204011]
41. Ready N, Jänne PA, Bogart J, Dipetrillo T, Garst J, Graziano S, et al. Chemoradiotherapy and gefitinib in stage II non-small cell lung cancer with epidermal growth factor and KRAS mutational analysis: cancer and leukemia group B (CALEB) 30106, a CALGB-stratified phase II trial. J Thorac Oncol. 2010; 5:1382–1390. [PubMed: 20686428]
42. Faber AC, Wong KK, Engelman JA. Differences underlying EGFR and HER2 oncogene addiction. Cell Cycle. 2010; 9:851–852. [PubMed: 20160489]
43. Gomez HL, Doval DC, Chavez MA, Ang PC, Aziz Z, Nag S, et al. Efficacy and safety of lapatinib as first-line therapy foRErbB2-amplified locally advanced or metastatic breast cancer. J Clin Oncol. 2008; 26:2999–3005. [PubMed: 18458039]
44. Sun Q, Ming L, Thomas SM, Wang Y, Chen ZG, Ferris RL, et al. PUMA mediates EGFR tyrosine kinase inhibitor-induced apoptosis in head and neck cancer cells. Oncogene. 2009; 18:2348–2357. [PubMed: 19421143]
45. Certo M, Del Gaizo Moore V, Nishino M, Wei G, Korsmeyer S, Armstrong SA, et al. Mitochondria primed by death signals determine cellular addiction to antiapoptotic BCL-2 family members. Cancer Cell. 2006; 9:351–365. [PubMed: 16697956]
46. Tse C, Shoemaker AR, Adickes J, Anderson MG, Chen J, Jin S, et al. ABT-263: a potent and orally bioavailable Bcl-2 family inhibitor. Cancer Res. 2008; 68:3421–3428. [PubMed: 18451170]
47. Faber AC, Chiles TC. Inhibition of cyclin-dependent kinase-2 induces apoptosis in human diffuse large B cell lymphomas. Cell Cycle. 2007; 6:2982–2989. [PubMed: 18156799]
48. Faber AC, Dufort FJ, Blair D, Wagner D, Roberts MF, Chiles TC. Inhibition of phosphatidylinositol 3-kinase-mediated glucose metabolism coincides with reseveratrol-induced cell cycle arrest in human diffuse large-B cell lymphomas. Biochem Pharm. 2006; 72:1246–1256. [PubMed: 16979140]
49. Turke AB, Zejnullahu K, Wu YL, Song Y, Dias-Santagata D, Lifshits E, et al. Preexistence and clonal selection of MET amplification in EGFR mutant NSCLC. Cancer Cell. 2010; 17:77–88. [PubMed: 20129249]
50. Dias-Santagata D, Akhavanfard S, David SS, Vernovsky K, Kuhlmann G, Boisvert SL, et al. Rapid-targeted mutational analysis of human tumours: a clinical platform to guide personalized cancer medicine. EMBO Mol Med. 2010; 2:146–158. [PubMed: 20432502]
51. Watanabe H, Yamamoto S, Kunitoh H, Sekine I, Yamamoto N, Ohe Y, et al. Tumor response to chemotherapy: the validity and reproducibility of RECIST guidelines in NSCLC patients. Cancer Sci. 2003; 11:1015–1020. [PubMed: 14611681]

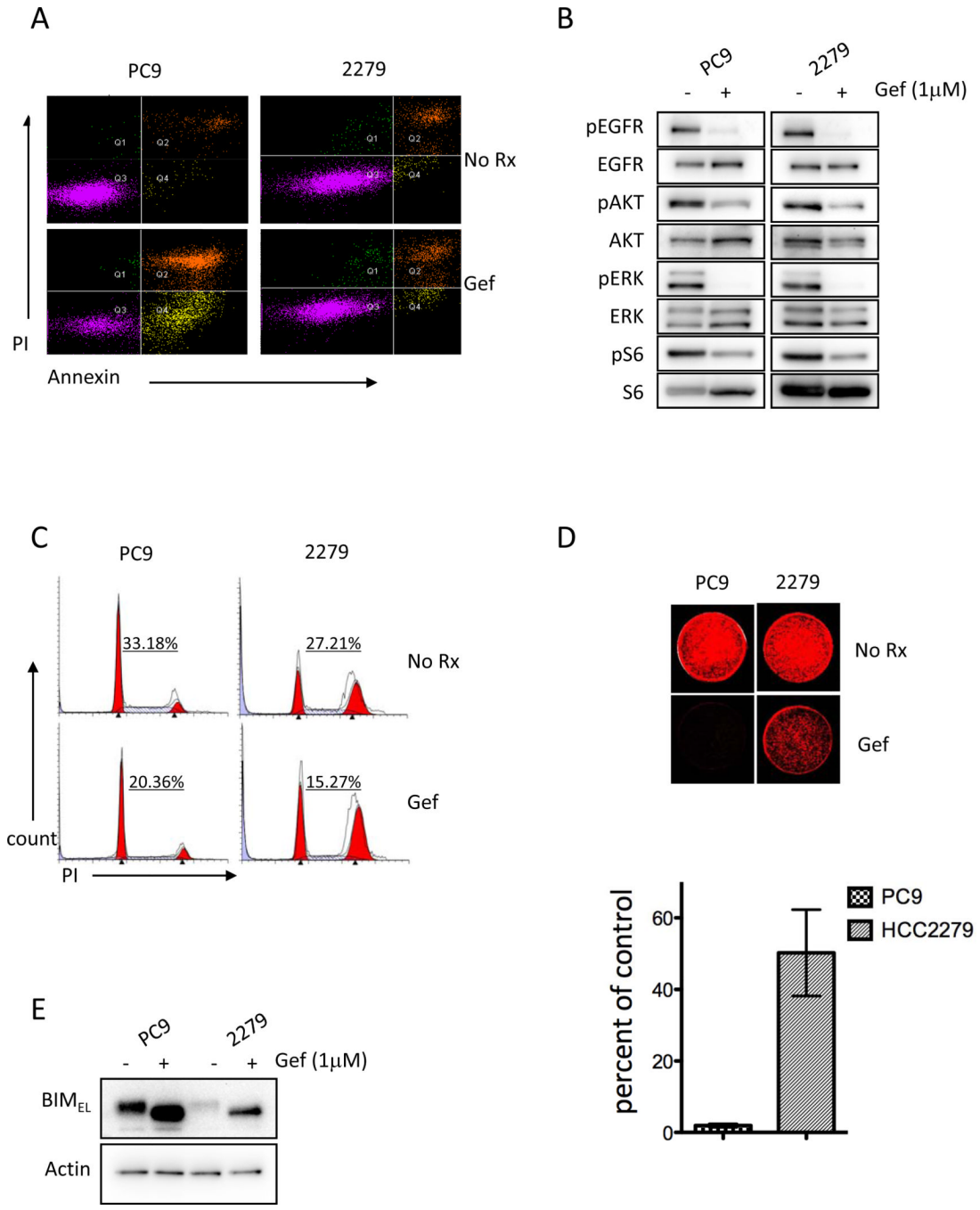

Figure 1. Higher basal BIM expression is associated with more robust apoptosis, but not cell cycle arrest, in response to TKI in *EGFR* mutant lung cancers

(A) *EGFR* mutant exon 19 deletion non-small cell lung cancers (NSCLC) cell lines PC9 and HCC2279 were treated with (+) or without (−) 1μM TKI (gefitinib) for 72 hours and stained with propidium iodide (PI) and Annexin V and analyzed by FACS to quantify annexin positive cells. Measurements of apoptosis at 24 and 48 hours are shown in Sup. Table 2. (B) The cell lines were treated as above for 24 hours and lystates were probed with the indicated antibodies. (C) The cell lines were treated as above for 24 hours and cell cycle distribution was determined by propidium iodide staining followed by FACS analyses. The percent of cells in S Phase is indicated. (D) The cell lines were treated as above with fresh media and

drug replenished every 72 hours until the vehicle control-treated (No Rx) plate grew to confluency. At that time both vehicle-treated and drug-treated plates were stained with the nuclear acid stain, SYTO60. A representative plate is shown (*upper panel*). The percent of TKI-treated cells that survived are shown (*lower panel*). Error bars are +/− S.D. of the mean of three experiments. (E) The cell lines were treated with 1μM gefitinib for 24 hours and lysates were probed with the antibodies against BIM and Actin.

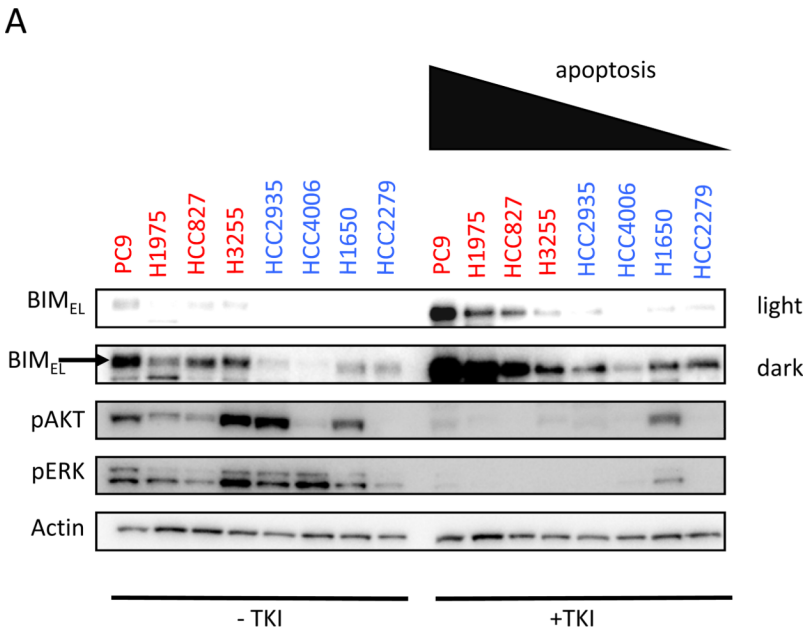

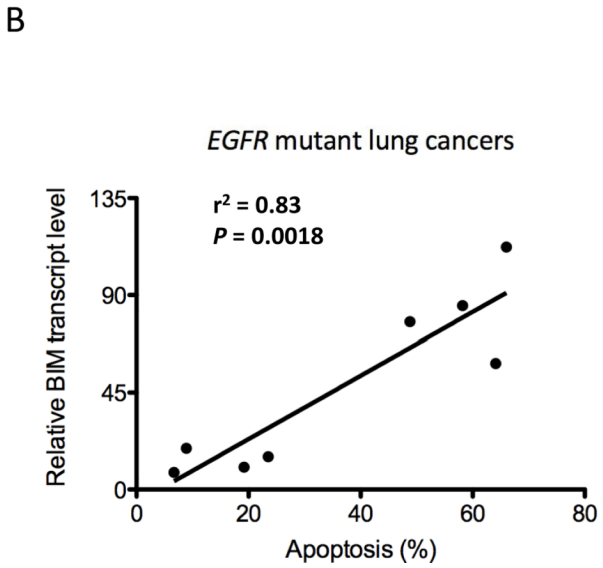

Figure 2. Greater induction of apoptosis following EGFR TKI treatment correlates with higher basal BIM expression across a panel of *EGFR* mutant lung cancers

(A) The indicated *EGFR* mutant lung cancer cell lines were treated with (+ TKI) or without (−TKI) 1μM gefitinib (2μM CL-387,785 for H1975 cells) for 24 hours and lysates were probed with the indicated antibodies (B) BIM RNA levels were quantified by qRT-PCR, normalized to β-Actin, and plotted against the amount of apoptosis induced by the TKI (over vehicle-control) as determined by annexin FACS. Both RNA values and apoptosis are the mean of at least three experiments (see Sup. Table 1). For the linear regression analysis, the r^2 value was 0.83 and P= 0.0018.

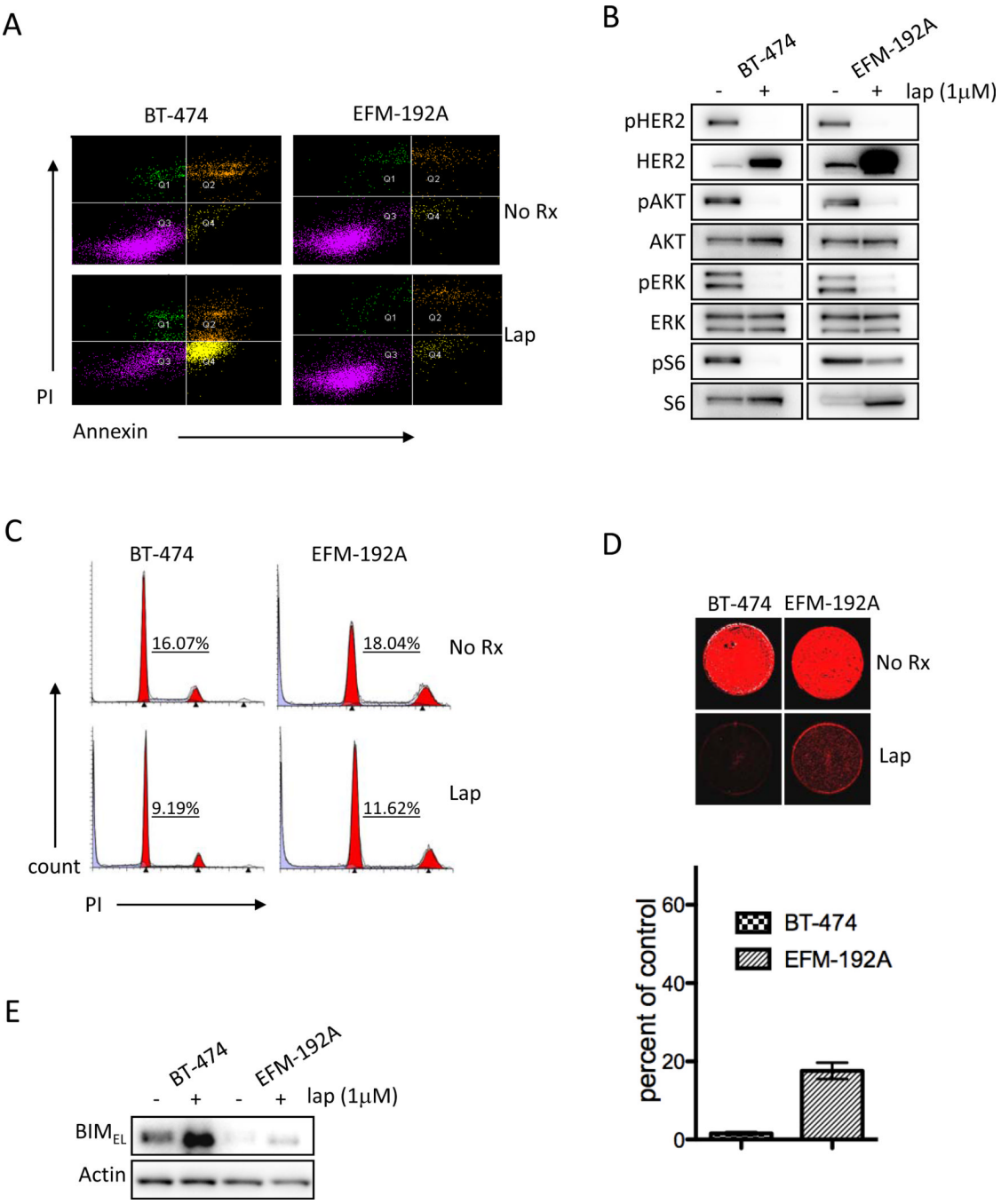

Figure 3. Higher basal BIM expression is associated with more robust apoptosis, but not cell cycle arrest, in response to TKI in *HER2* amplified cancers

(A) *HER2* amplified breast cancer cells BT-474 and EFM-192A were treated with (+) or without (−) 1μM TKI (lapatinib) for 72 hours and stained with propidium iodide (PI) and Annexin V and analyzed by FACS to quantify annexin positive cells. (B) The cell lines were treated as above for 24 hours and lystates were probed with the indicated antibodies. (C) The cell lines were treated as above for 24 hours and cell cycle distribution was determined by propidium iodide staining followed by FACS analyses. The percent of cells in S Phase is indicated. (D) The cell lines were treated as above with fresh media and drug replenished every 72 hours until the vehicle control-treated (No Rx) plate grew to confluency. At that

time both vehicle-treated and drug-treated plates were stained with the nuclear acid stain, SYTO60. A representative plate is shown (*upper panel*). The percent of TKI-treated cells that survived are shown (*lower panel*). Error bars are +/−S.D. of the mean of three experiments. (E) The cell lines were treated with 1μM lapatinib for 24 hours and lystates were probed with the antibodies against BIM and Actin.

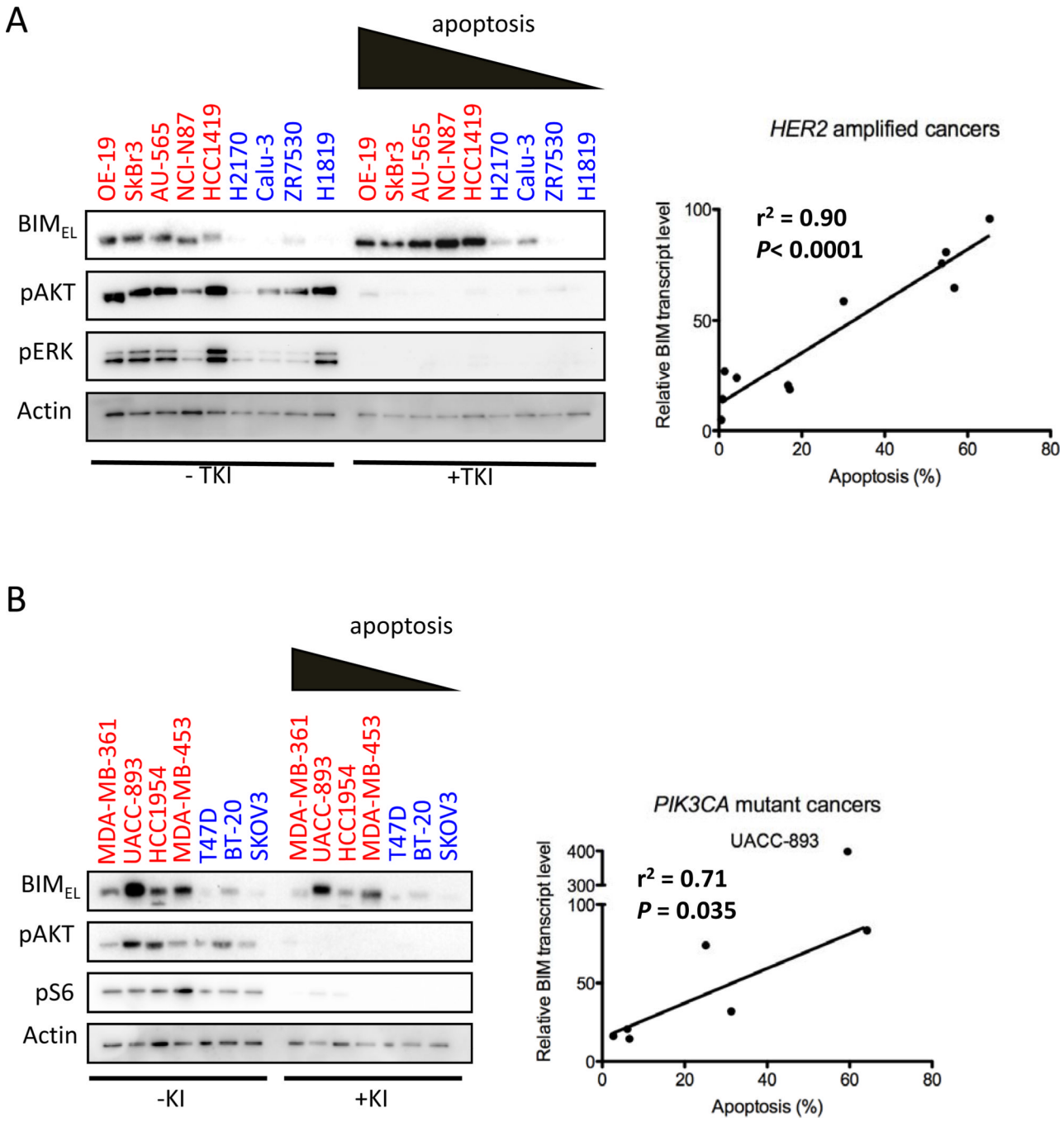

Figure 4. Greater induction of apoptosis correlates with higher basal BIM expression across a panel of *HER2* amplified cancers and *PIK3CA* mutant cancers following treatment with HER2 and PI3K inhibitor treatment respectively

(A) *Left panels. HER2* amplified cancer cell lines were treated with (+ TKI) or without (- TKI) (1μM lapatinib) for 24 hours and lysates were probed with the indicated antibodies. *Right panel.* BIM RNA levels were quantified by qRT-PCR, normalized to β-Actin, and plotted against the amount of apoptosis induced by the TKI (over vehicle-control) as determined by annexin FACS. Both RNA values and apoptosis are the mean of at least three experiments (see Sup. Table 1). For the linear regression analysis, the r^2 value was 0.90 and $P< 0.0001$. Please note the BT-474 and EFM-192A cells (Fig. 3) were included in the RNA

analysis. (B) *Left panels.* The indicated *PIK3CA* mutant cancers were treated with (+ KI) or without (− KI) 200nM NVP-BEZ235 for 24 hours and lysates were probed with the indicated antibodies. *Right panel.* BIM RNA levels were quantified by qRT-PCR, normalized to β-Actin, and plotted against the amount of apoptosis induced by NVP-BEZ235 (over vehicle control) as determined by annexin FACS. Both RNA values and apoptosis are the mean of at least three experiments (see Sup. Table 1). For the linear regression analysis, the r^2 value was 0.71 and $P = 0.035$. The UACC-893 cells were excluded from the analysis.

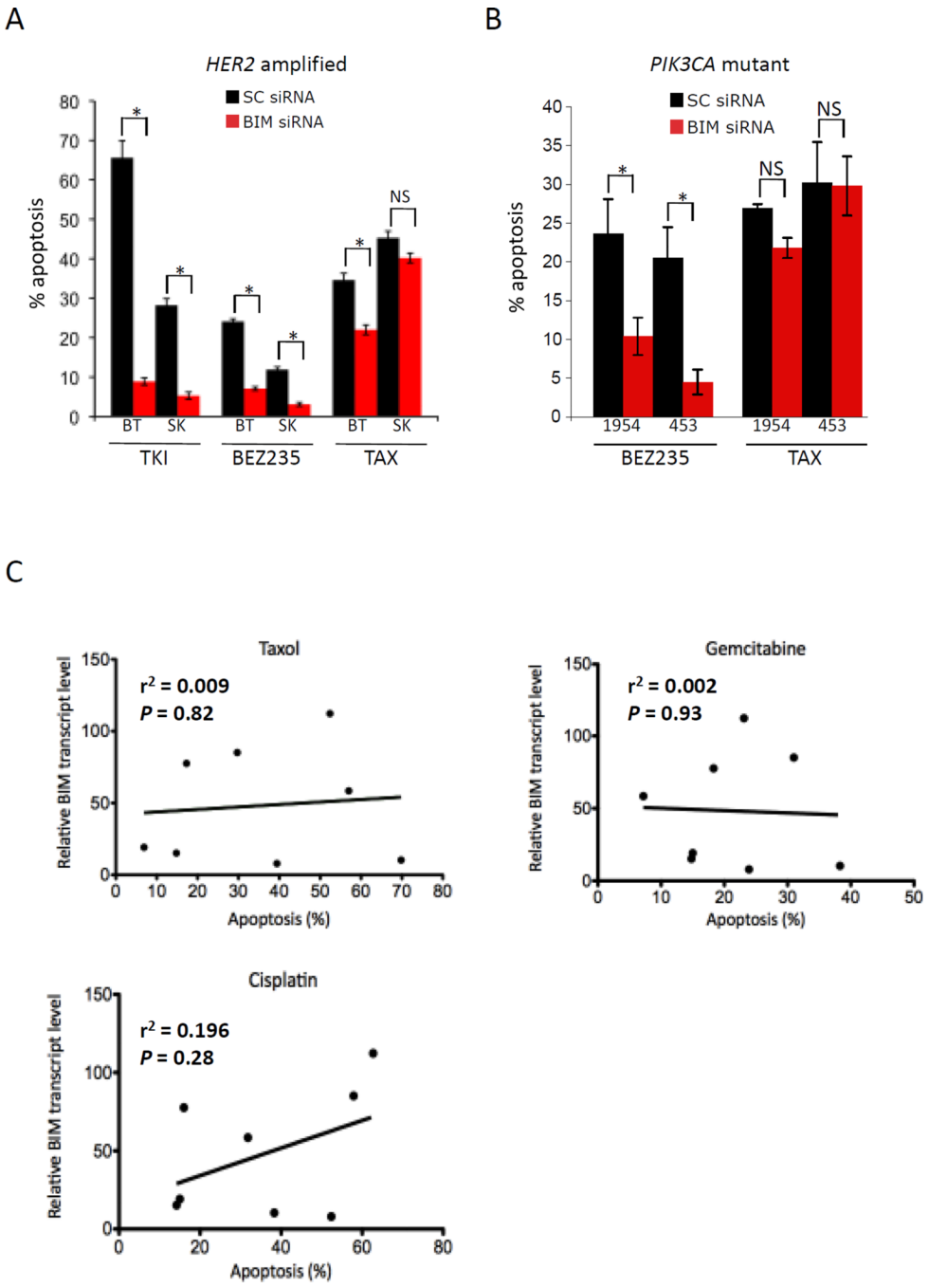

Figure 5. Loss of BIM protects *EGFR* mutant, *HER2* amplified and *PIK3CA* mutant cancers from targeted therapy-induced apoptosis, but not from cytotoxic chemotherapy-induced apoptosis

(A) *HER2* amplified or (B) *PIK3CA* mutant cancer cell lines were transiently transfected with either scrambled (SC) or BIM siRNA for 24 hours and then split for the drug treatments. The next day cells were treated with vehicle control, 1μM lapatinib, 200nM NVP-BEZ235 (BEZ235) or the microtubule poison taxol (TAX, 200nM) for 48 hours and stained with propidium iodide and annexin V and analyzed by FACS. Bars represent average percent of apoptosis drug treatment over vehicle control. Error bars are −/+ S.D. of the mean of three experiments. * indicates significance ($P < 0.05$) between two treatments as

determined by a Student's *t* test and NS = not significant. (C) RNA levels of BIM (normalized to β-Actin) from *EGFR* mutant cancer cell lines were plotted against the amount of apoptosis induced by 200nM taxol, 500nM gemcitabine, or 10μM cisplatin minus vehicle control (72 hours) as determined by annexin FACS. The linear regression analysis showed no significant correlation between cytotoxicity of any of the treatments and BIM RNA levels.

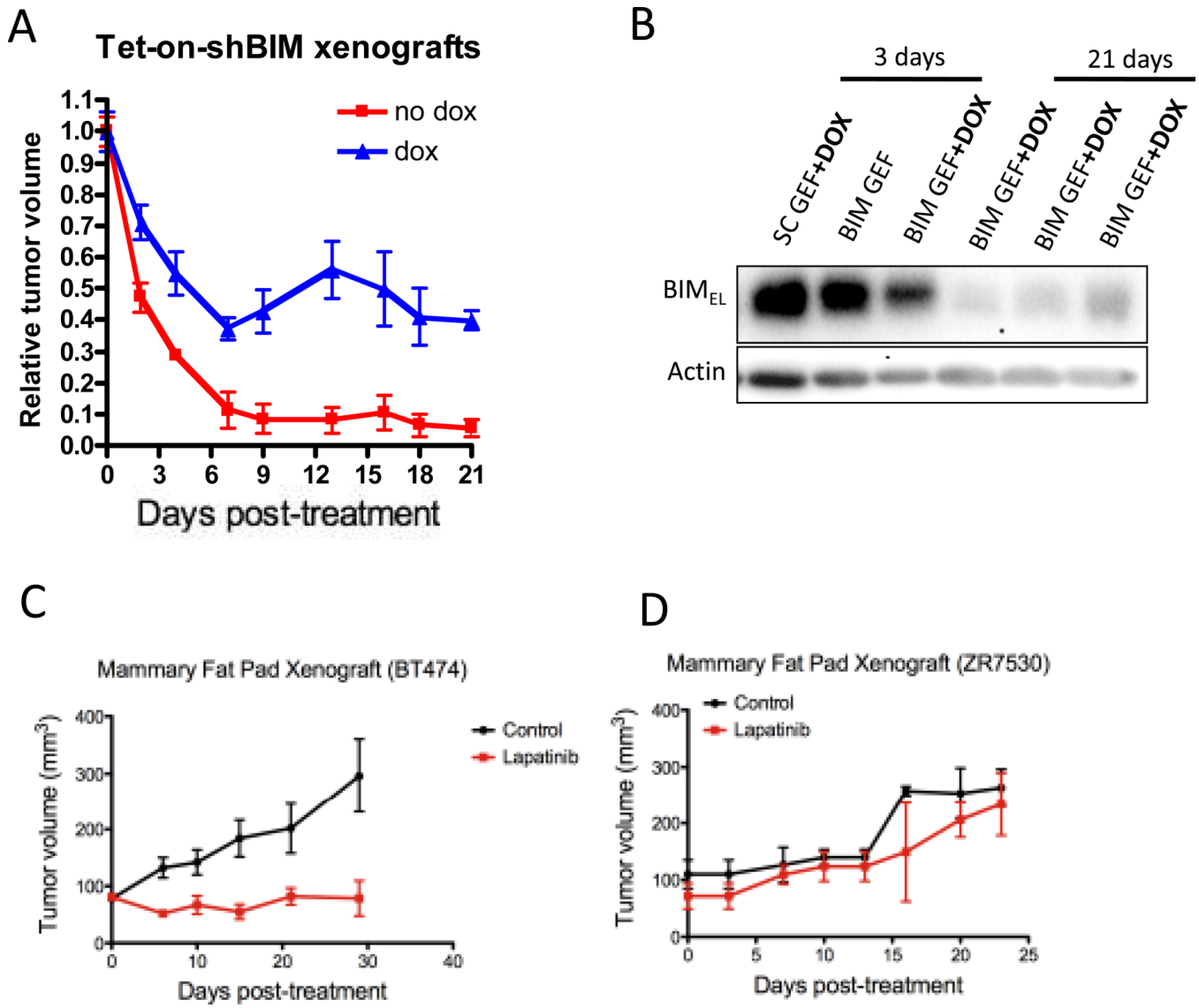

Figure 6. The efficacy of targeted therapies in vivo is dependent on induction of apoptosis

(A) HCC827 cells carrying a doxycycline (DOX) inducible short hairpin (SH) targeting BIM were injected into 6–8 week-old nude mice. When tumors reached approximately 100mm^3, half the mice were switched to DOX chow. When tumors reached approximately 750mm^3 all the mice were treated with gefitinib (35mg/kg) once daily for 21 days and the average tumor measurements of the two groups are shown. Error bars are +/– S.E.M. of the mean tumor measurement of each treatment group.

(B) HCC827 cells carrying a plasmid with a DOX inducible short hairpin (SH) sequence targeting either a scrambled (SC) or a BIM sequence, were injected into 6–8 week-old nude mice. Tumors were treated as indicated and were harvested at the indicated times after gefitinib treatement. Lysates were prepared and probed with the indicated antibodies. (C and D) 6–8 week old female mice were injected with BT-474 or ZR7530 *HER2* amplified breast cancer cells into the mammary fat pad following ovariectomy. When tumors approached 125mm3 they were treated with vehicle or 100mg/kg lapatinib and tumor volume was measured for ~ 30 days. Error bars are +/− S.E.M. of the mean tumor measurement of each treatment group.

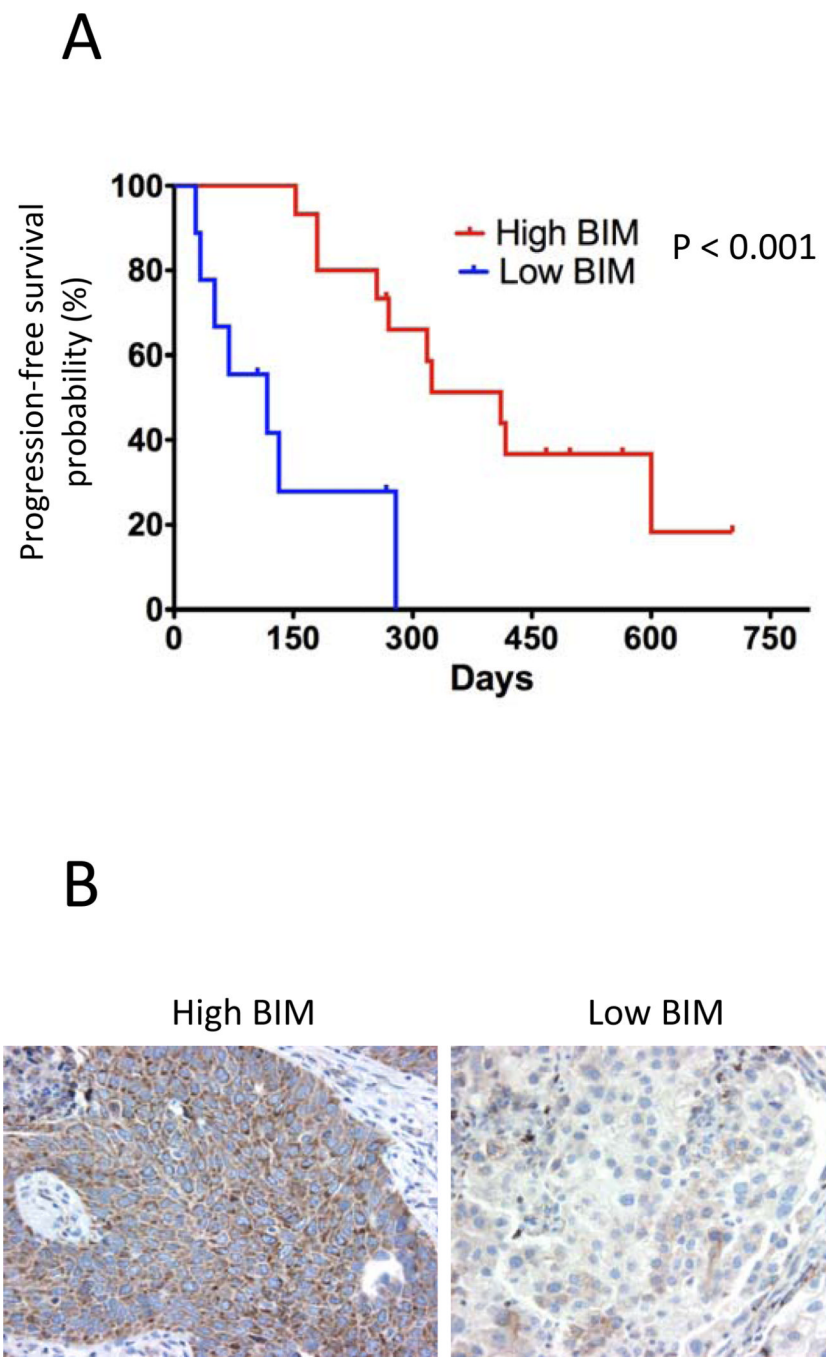

Figure 7. BIM expression predicts the response of patients with *EGFR* mutant lung cancers

(A) Tumor samples from EGFR TKI-naïve patients with *EGFR* mutant lung cancers were extracted prior to treatment and assayed for BIM RNA expression, normalized to β-actin RNA, were separated by high BIM (n=15, relative BIM RNA >45) and low BIM (n=9, relative BIM RNA<30). Progression free survival was calculated with the Kaplan-Meier method and significance assessed via the log rank test (P <0.001). (B) Immunohistochemistry (IHC) of two samples. High BIM expressing cancer (left) and low BIM expressing cancer (right).